Supplement of Atmos. Meas. Tech., 14, 6335–6355, 2021
https://doi.org/10.5194/amt-14-6335-2021-supplement

Atmospheric Measurement Techniques
Open Access
EGU

Supplement of

Determination of the multiple-scattering correction factor and its cross-sensitivity to scattering and wavelength dependence for different AE33 Aethalometer filter tapes: a multi-instrumental approach

Jesús Yus-Díez et al.

Correspondence to: Jesús Yus-Díez (jesus.yus@idaea.csic.es)

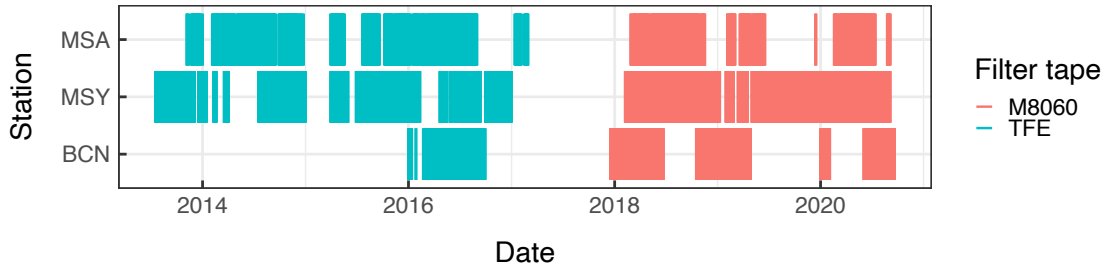

Figure S1. Multiple scattering parameter (C) availability for both M8060 and TFE filter tape at BCN, MSY and MSA measurement supersites.

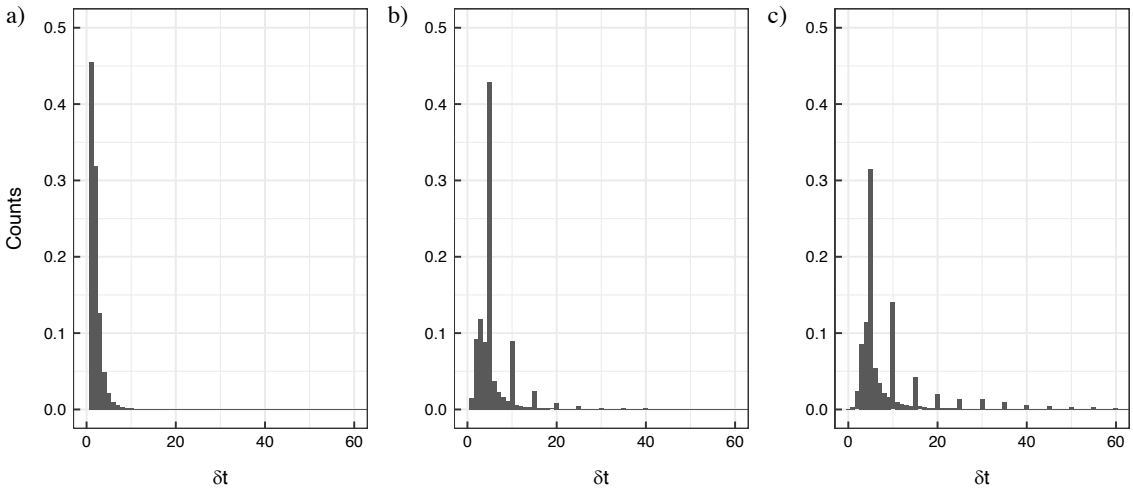

Figure S2. Normalized count distribution of the measurement timestamp, δt in minutes for a) BCN, b) MSY, and c) MSA. Time measurement resolution was set to 1 min when possible, in b) and c) the 5 min spikes are due to a measurement time resolution of 5 min during a certain period of time.

INSTRUMENT	STATION	TIMESTAMP
AE33	BCN	1 min
	MSY	1 min
	MSA	1 min
MAAP	BCN	1 min
	MSY	1 min
	MSA	1 min
NEPHELOMETER	BCN	1 min
	MSY	5 min (2013-February February 2017); 1 min (February 2017-2020)
	MSA	5 min (2013-February February 2017); 1 min (February 2017-2020)

Table S2. Timestamp of the measurement for each instrument, AE33, MAAP and nephelometer, for each station.

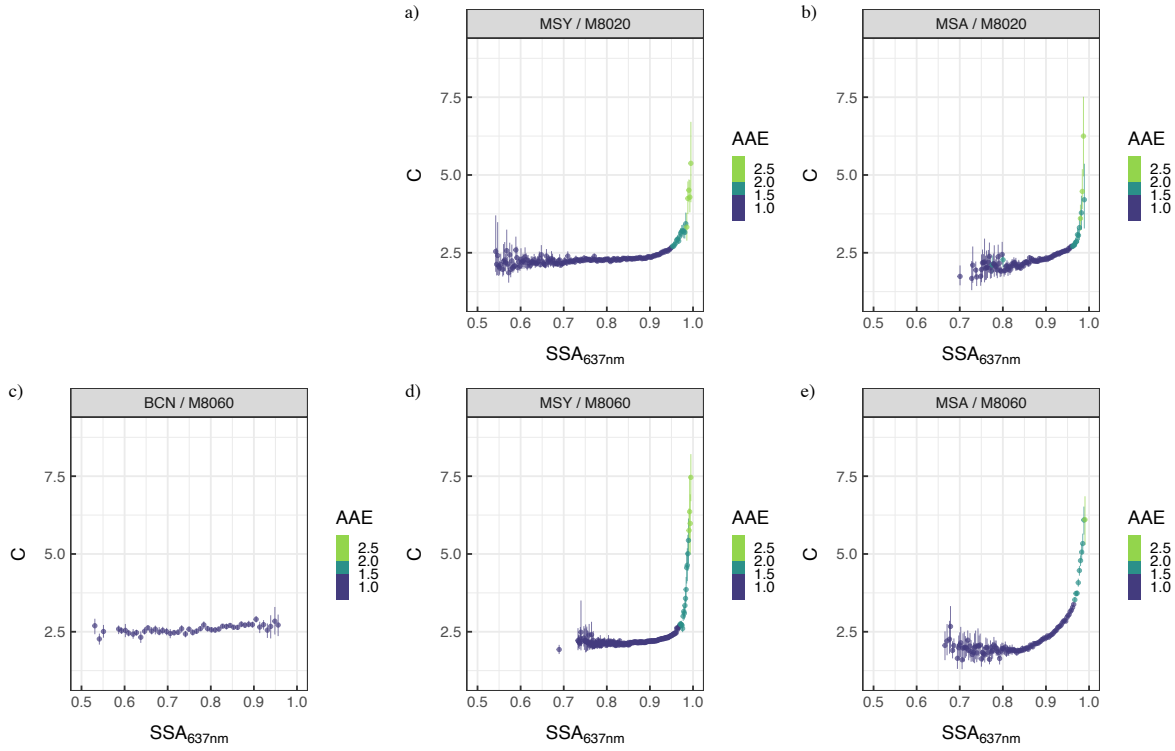

Figure S3. Multiple scattering parameter (C) dependence on the single scattering albedo (SSA) for the TFE-coated glass (upper panel) and the M8060 filter tape (lower panel) at: BCN (c), MSY (a,d) and MSA (b,e) measurement supersites as a function of the absorption Ångström exponent (AAE).

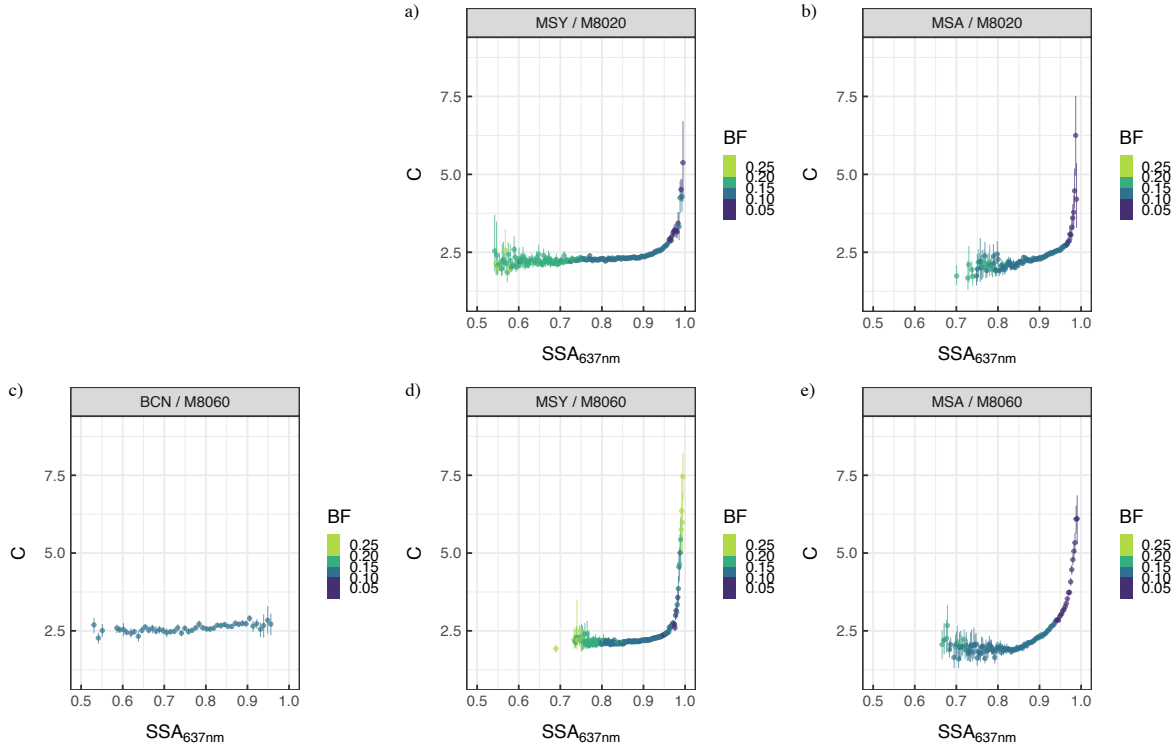

Figure S4. Multiple scattering parameter (C) dependence on the single scattering albedo (SSA) for the TFE-coated glass (upper panel) and the M8060 filter tape (lower panel) at: BCN (c), MSY (a,d) and MSA (b,e) measurement supersites as a function of the backscattered fraction at (BF).

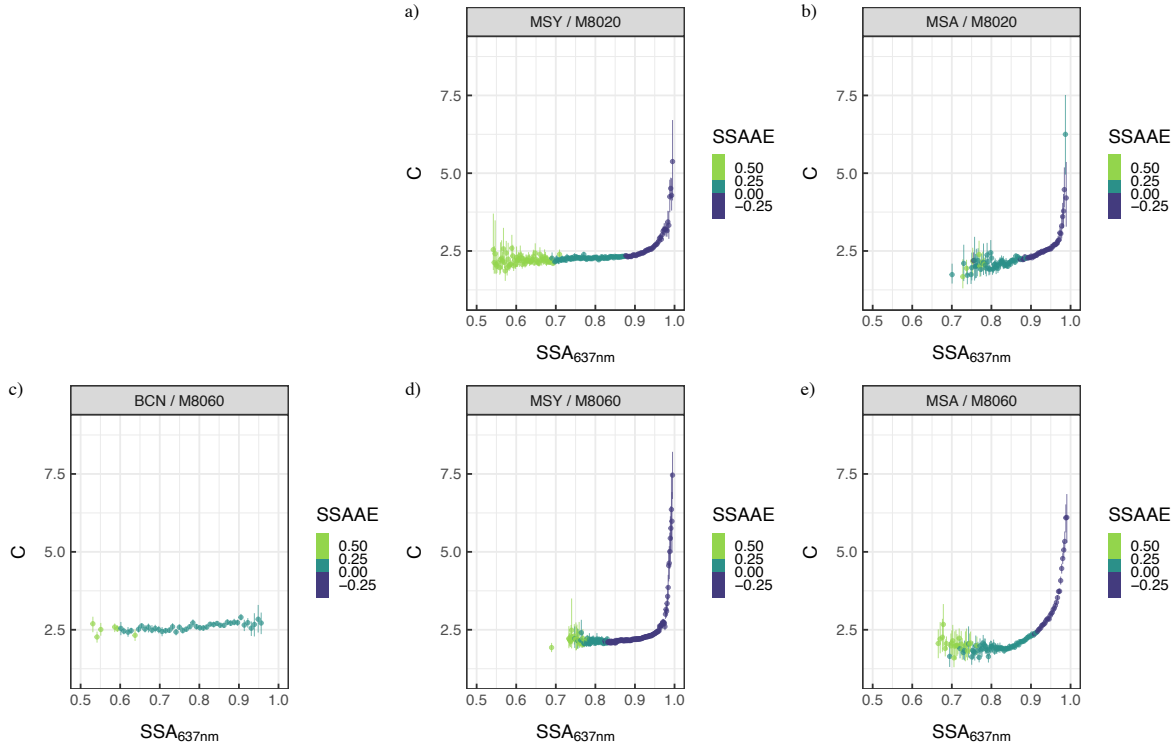

Figure S5. Multiple scattering parameter (C) dependence on the single scattering albedo (SSA) for the TFE-coated glass (upper panel) and the M8060 filter tape (lower panel) at: BCN (c), MSY (a,d) and MSA (b,e) measurement supersites as a function of the single-scattering albedo Ångström exponent (SSAAE).

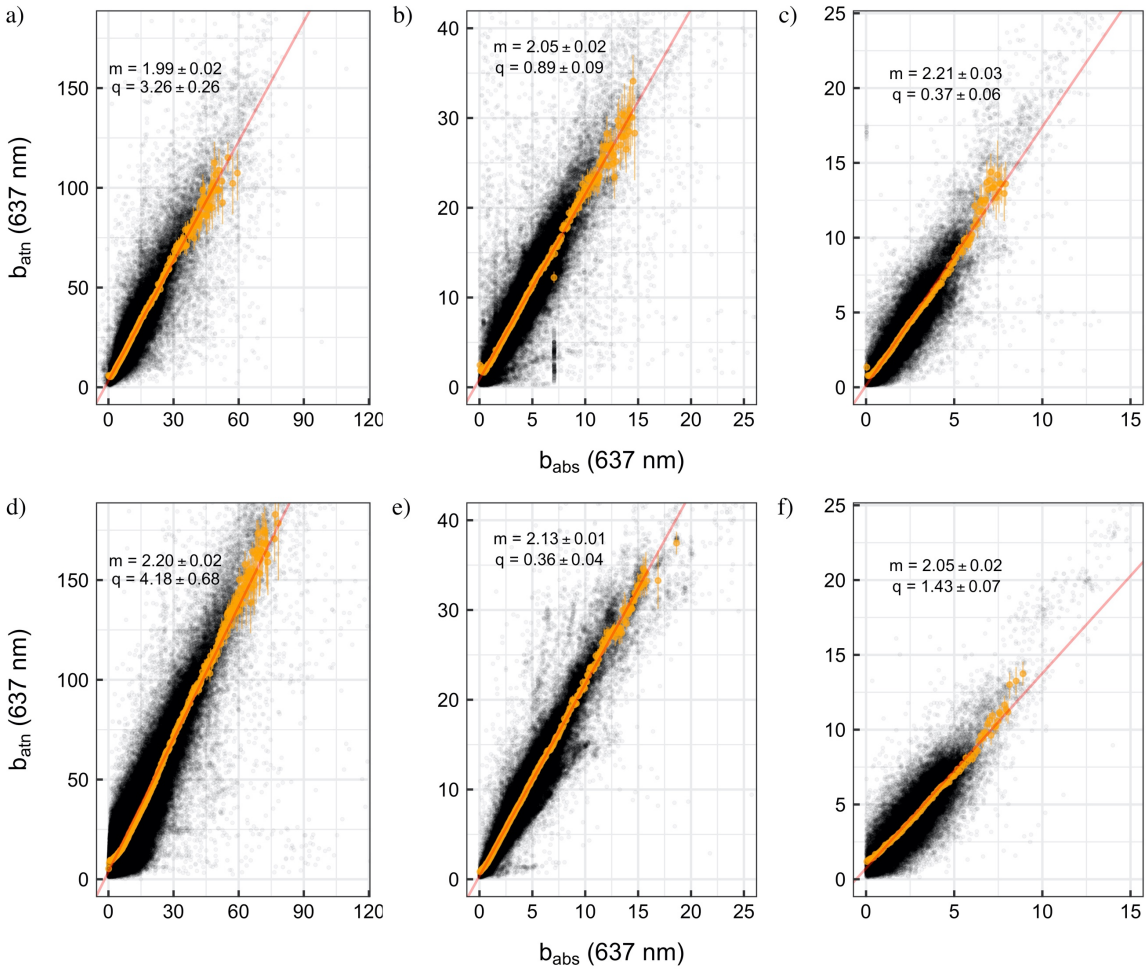

Figure S6. Scatter-plot of the binned AE33 attenuation coefficient (b_{atn} (637 nm)) vs MAAP absorption coefficient b_{abs} (637 nm)) where the slope of the Deming regression, m, represents the multiple-scattering parameter C, and q is the intercept of the regression, for the TFE-coated glass filter tape (upper panels) and M8060 filter tape (lower panels) for BCN (a,d), MSY (b,e) and MSA (c,f). The non-zero intercept, q, is indicative of the additional signal due to the cross-sensitivity to scattering of particles within the filter.

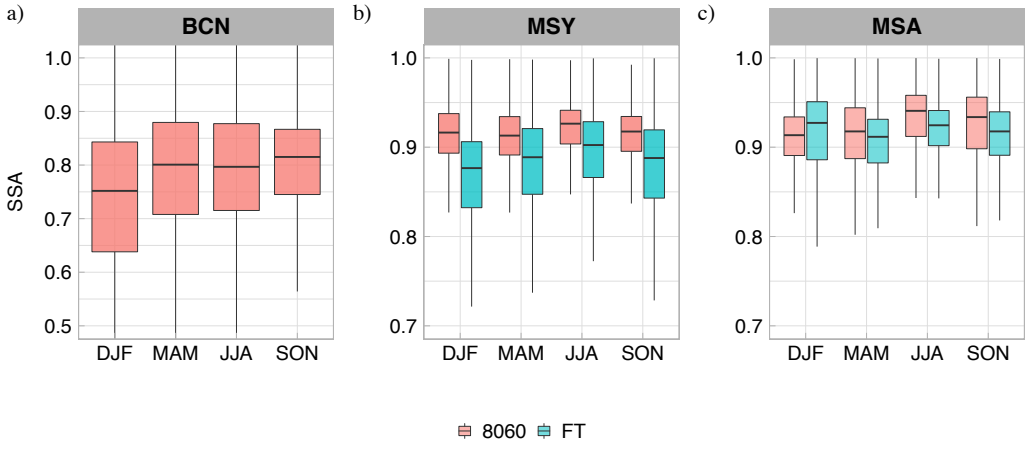

Figure S7. Seasonal evolution of the SSA at a) BCN, b) MSY and c) MSA measurement stations for both M8020 and M8060 filter tapes. The box plot boxes show the range between the first and third quartile (IQR) with the median value for each season distribution represented by the inner line; the maximum whisker length is proportional to 1.5·IQR.

a)

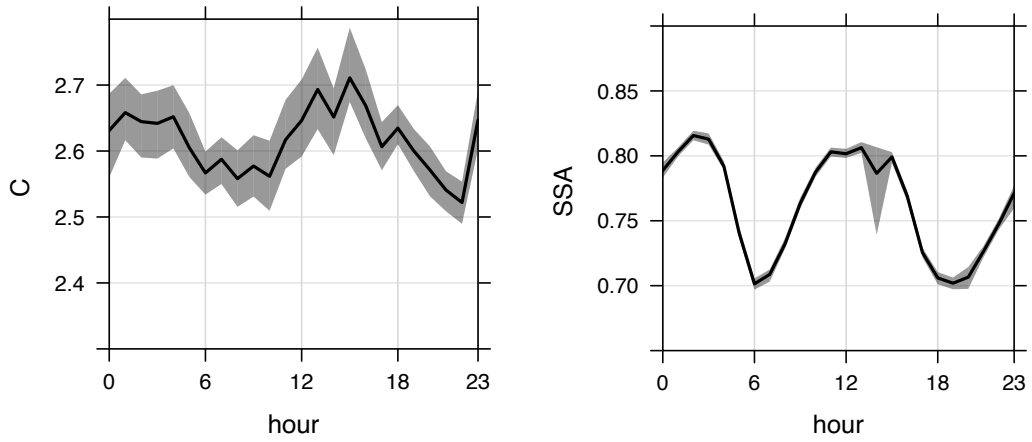

b):

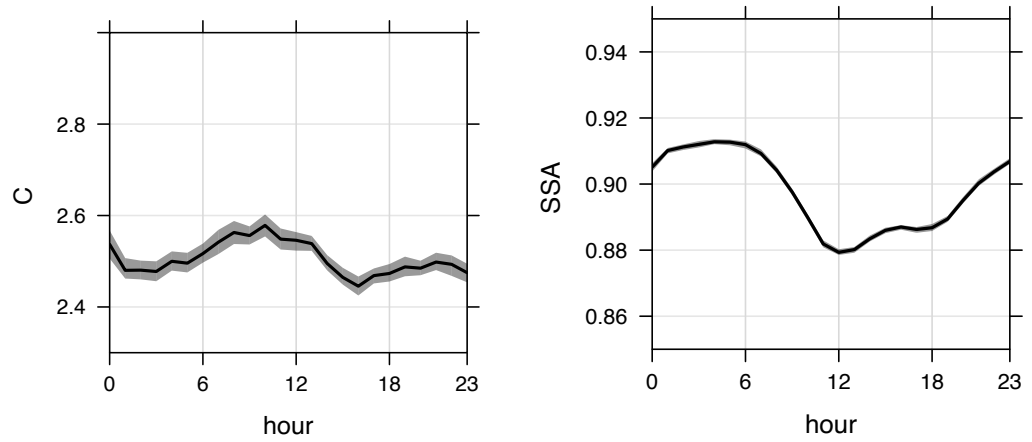

c):

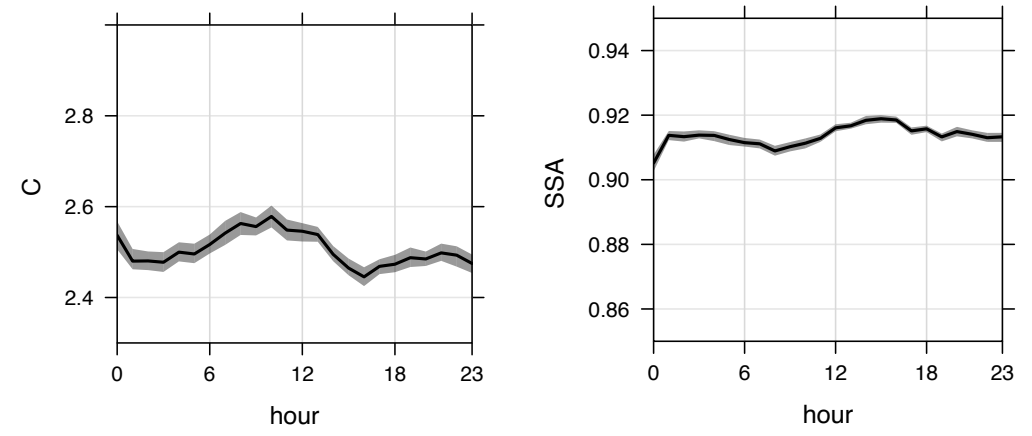

Figure S8. Diel evolution of the C and the SSA actor at a) BCN, b) MSY and c) MSA measurement stations. The measurement period of this cycles corresponds to all the available dataset for both M8020 and M8060 filter tapes (cf. Fig. S1).

	$C_{PP\_UniMI}(\lambda)$						
	370 nm	**470 nm**	**520 nm**	**590 nm**	**660 nm**	**880 nm**	**950 nm**
BCN	3.36	3.26	3.22	3.24	3.21	3.19	3.31
MSY	2.68	2.67	2.72	2.77	2.79	2.62	6.67
MSA	3.47	3.48	3.58	3.71	3.87	4.05	4.03

Table S2. Multiple scattering factor (C) at each AE33 measuring wavelength obtained using the absorption coefficient from the PP_UniMI polar photometer for BCN, MSY and MSA measurement supersites.

	$C_{PaM}(\lambda)$						
	370 nm	**470 nm**	**520 nm**	**590 nm**	**660 nm**	**880 nm**	**950 nm**
BCN	2.82	2.78	2.75	2.73	2.72	2.69	2.83
MSY	2.32	2.33	2.42	2.46	2.47	2.26	2.32
MSA	2.82	2.85	2.91	3.03	3.09	3.22	3.24

Table S3. Multiple scattering factor (C) at each AE33 measuring wavelength obtained using the absorption coefficient from the PP_UniMI polar photometer working as MAAP (PaM) for BCN, MSY and MSA measurement supersites.

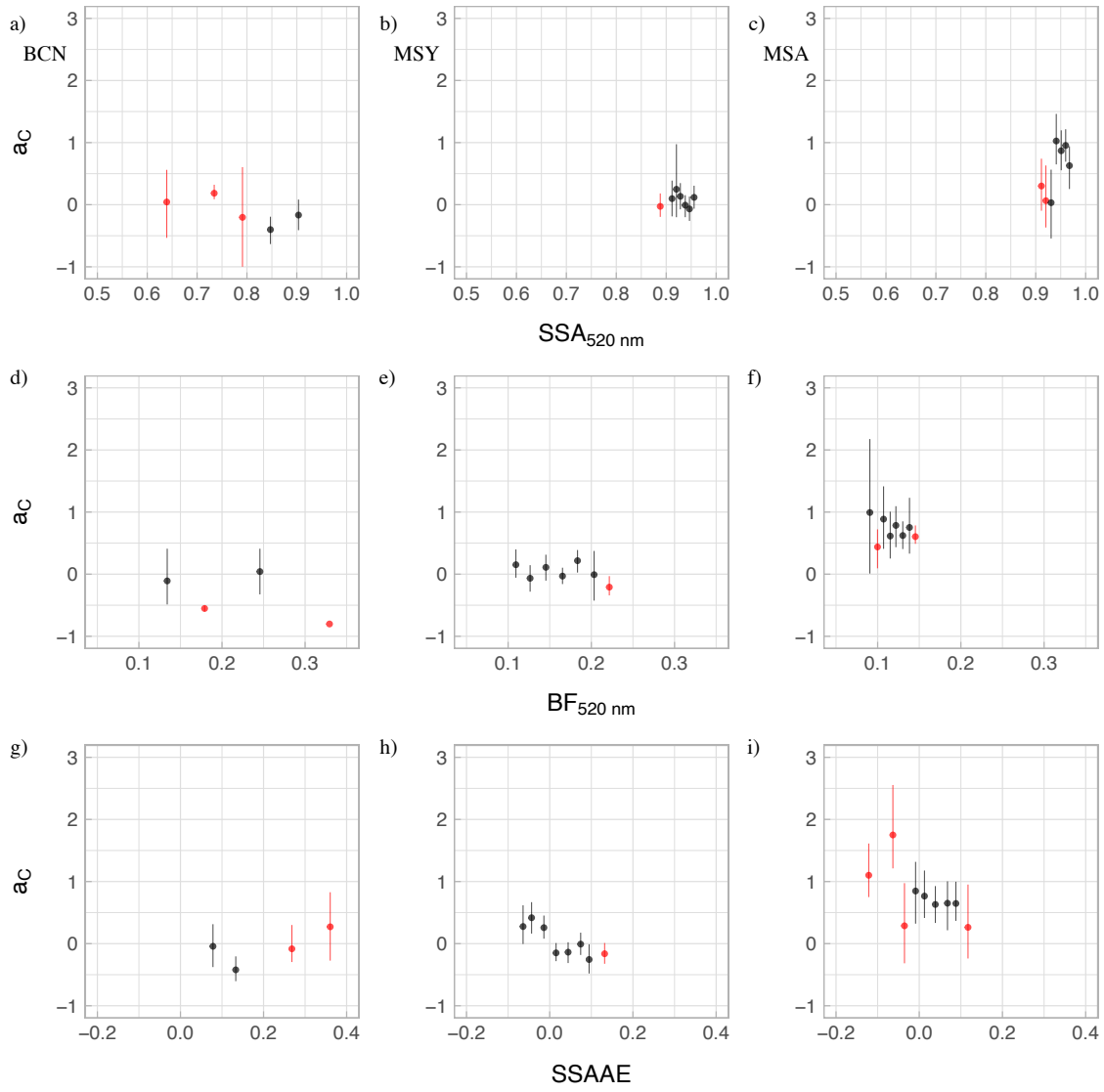

Figure S9. Relationship between the slope of the factor C and the wavelength, a_C, and the single-scattering albedo at 520 nm (SSA_{520nm}), the backscatter fraction (BF_{520nm}), and the single-scattering albedo Ångström exponent (SSAAE) at BCN (left panel), MSY (middle panel) and MSA (right panel) measurement stations. The values of a_C (y-axis) for a given station changed depending on the dependent variable (x-axis) considered due to the method employed for binning the data. Here we used the Freedman-Diaconis rule to define the bin width that can, consequently, include different data points depending on the variable considered. The red points show bins with a number of measurements which range between 2 and 5 data points.

	AAE	
	$\boldsymbol{C(const)}$	$\boldsymbol{C(\lambda)}$
BCN	1.19 ± 0.15	1.17 ± 0.15
MSY	1.27 ± 0.12	1.25 ± 0.12
MSA	1.19 ± 0.07	1.35 ± 0.07

Table S4. Mean values of the absorption Ångström exponent (AAE) for the sensitivity analysis performed in Fig. 3 on the AAE obtained using a wavelength-dependent C ($C(\lambda)$) in comparison with an AAE obtained using a constant C, C(const), parameter.

a)

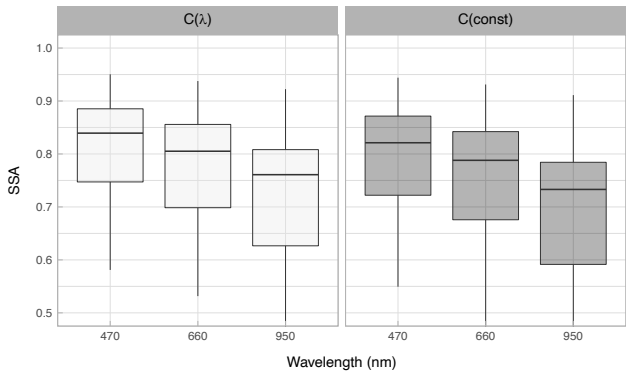

b)

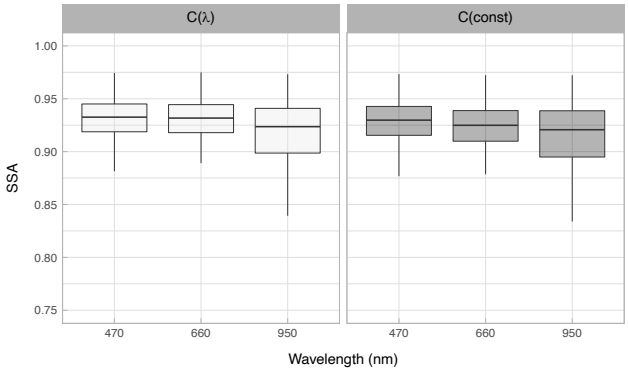

c)

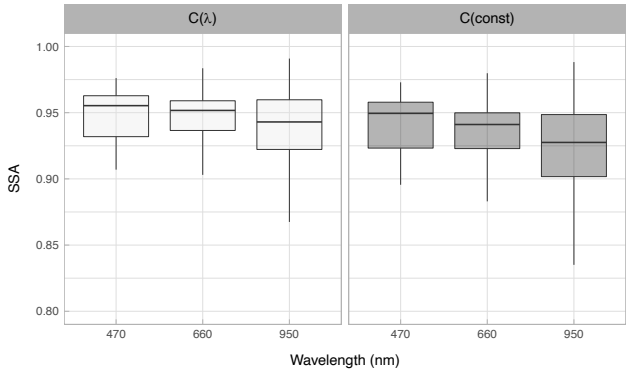

Figure S10. Sensitivity analysis of the single scattering albedo (SSA) on the wavelength-dependent C (C(λ)) in comparison with an SSA at 3 wavelengths (470, 660 and 950 nm) obtained using a constant C parameter (C(const)) for a) BCN, b) MSY and c) MSA measurement stations.